

# Effect of single vanes on turbulent flow

Sara Ahmadi Adli<sup>1</sup>, Akram Abbaspour<sup>1</sup>, Ali Hosseinzadeh Dalir<sup>1</sup> and Javad Parsa<sup>1</sup>

<sup>1</sup> University of Tabriz, Faculty of Agriculture, Department of Water Science and Engineering, 29 Bahman Blvd, 5166616471, Tabriz, Iran

**Corresponding author:**

Sara Ahmadi Adli  
[saraahmadiadli@yahoo.com](mailto:saraahmadiadli@yahoo.com)

**Received:**  
October 18, 2023

**Accepted:**  
January 15, 2024

**Published:**  
April 4, 2024

**Citation:**

Ahmadi Adli, S.; Abbaspour, A.;  
Hosseinzadeh Dalir, A.; Parsa, J.  
Effect of single vanes on turbulent  
flow.  
*Advances in Civil and  
Architectural Engineering*,  
2024, 15 (28), pp. 76-86.  
<https://doi.org/10.13167/2024.28.6>

**ADVANCES IN CIVIL AND  
ARCHITECTURAL ENGINEERING  
(ISSN 2975-3848)**

Faculty of Civil Engineering and  
Architecture Osijek  
Josip Juraj Strossmayer University  
of Osijek  
Vladimira Preloga 3  
31000 Osijek  
CROATIA



**Abstract:**

In response to growing environmental and ecological awareness, eco-friendly in-stream structures such as vanes have been implemented in different parts of the world to enhance stream conditions. FLUENT (ANSYS) was used to perform three-dimensional large eddy simulation to investigate the effect of the vanes permeability rate on flow characteristics. To evaluate the numerical model accuracy, numerical and experimental free surface profiles compared. It is observed that simulated free surface profiles agree reasonably well with measured values. The effect of different permeability rates is obvious in the flow characteristics such as depth-averaged velocity distribution, tip velocity variations, formation of the secondary flows in the flow field, turbulent kinetic energy, and mean kinetic energy contours. On average, maximum velocity values in the flow field is 1,54 times the approach velocity. Tip velocity decreases up to 30,6 % for the 70,0 % permeable vane. Maximum turbulent kinetic energy and mean kinetic energy for the 70,0 % permeable vane decrease up to 58,0 % and 43,3 %, respectively. Generally significant velocity and flow pattern variations around the impermeable vane can be attributed to the local effect of the vane structure and channel cross sectional constriction in comparison to the permeable vanes.

**Keywords:**

eco-friendly structures; flow characteristics; large eddy simulation; permeability; vanes

## 1 Introduction

In the last few decades, river restoration projects have been mainly focused on natural functioning and biodiversity of the river system. In general, river restoration refers to the environmental and ecological aspects of the river engineering. Recently in-stream structures such as vanes, deflectors, W-weir, U-weir, cross vane and J-hook vanes have been implemented not only to protect river banks, stabilise river alignment and control river bed, but also to restore and rebuild natural habitat [1, 2]. Thus, in recent years' eco-friendly structures have been used to control bank erosion and improve river ecosystem [3]. Studies have been conducted to investigate the performance of the eco-friendly in-stream structures. In general, in-stream structures such as bank-attached vanes, permeable groins, cross vanes and W-weirs are developed is to overcome negative effects of the conventional structures on rivers ecosystem [4, 5].

Numerous studies have been conducted to investigate turbulent flow characteristics such as bed shear stress distribution, mean and turbulent flow pattern around groins [6-10]. Three-dimensional large eddy simulation (LES) model was used to analyse the flow pattern around non-submerged spur dike [11]. Velocity distributions, flow pattern and free surface fluctuations were investigated around a spur dike using FLUENT software and results obtained from the numerical model were compared with the experimental results [12]. Kang et al. [13] studied the effect of permeable groins (pile groins) on flow characteristics and downstream recirculation zone. In this study parameters such as tip velocity, maximum velocity and flow separation angle were investigated and results showed that as the permeability of the groins increased, effect of these structures on the flow field decreased. Fang et al. [14] used LES model to study the flow field around a non-submerged groin in a shallow open channel flow. Shen et al. [15] studied flow field and water level fluctuations around a permeable sheet of spur dike. In this study permeable spur dikes consisted of different number of permeable holes. Ferro et al. [16] investigated the effectiveness of a new river restoration technique in river bends, which is a combination of permeable groin and a triangular vane. They studied the scour hole characteristics and morphological changes and obtained results revealed that this new structure could provide a proper river bed and bank protection. Abdou et al. [17] employed LES model to study flow features in a 193° open channel bend. They investigated the velocity distributions and water depth variations. Iqbal et al. [18] used Reynolds stress model to simulate flow field around permeable rectangular spur dikes. They observed that the flow characteristics such as turbulent kinetic energy (TKE) and turbulent intensities decreased around permeable spur dike. Haider et al. [19] used FLUENT software to study flow field around permeable spur dikes in an open channel. They investigated the flow characteristics such as velocity distribution, turbulent kinetic energy and turbulent intensity. Mostafa et al. [20] studied flow characteristics and velocity distribution around hybrid groins having different orientation angle and geometry. The obtained results revealed that these structures generally enhance the formation of the riparian habitats.

Most of the researches and previous works related to bank-attached vanes and groins have mainly focused on the local scour and morphological changes and few in detail studies have been conducted regarding the turbulent flow characteristics near and downstream these structures. This may be attributed to the limitations of the different numerical models or measurement tools. However, considering the effective performance of bank-attached vanes in controlling bank erosion and improving river conditions, more research is needed to understand the complex flow field around these structures.

Due to the relatively accurate simulation of the wakes and vortices, large eddy simulation model (LES) was used in this study to simulate the flow field around the bank-attached rectangular vanes over a flatbed condition to understand the effect of different permeability rates on flow characteristics.

## 2 Methodology

### 2.1 Numerical Model and Computational Domain Setup

In large eddy simulation (LES) turbulence model, flow field is simulated by solving the Navier-Stokes equations. In LES model, large scale eddies are resolved directly, while small scale eddies are modelled. Governing equations are expressed as follows:

$$\frac{\partial \bar{u}_i}{\partial x_i} = 0 \quad (1)$$

$$\frac{\partial \bar{u}_i}{\partial t} + \frac{\partial (\bar{u}_i \bar{u}_j)}{\partial x_j} = -\frac{\partial \bar{p}}{\rho \partial x_i} + \nu \frac{\partial}{\partial x_j} \left( \frac{\partial \bar{u}_i}{\partial x_j} + \frac{\partial \bar{u}_j}{\partial x_i} \right) = -\frac{\partial \bar{p}}{\rho \partial x_i} + 2\nu \frac{\partial}{\partial x_j} \bar{S}_{ij} \quad (2)$$

In Eq. (2),  $\bar{p}$  is the filtered pressure field and the term  $(\bar{S}_{ij})$  is the rate-of-strain tensor evaluated using the filtered velocity. Due to the unknown unfiltered velocity field, it is difficult to determine the nonlinear filtered term  $(\bar{u}_i \bar{u}_j)$ , thus it needs to be modelled; the term can be split up as follows [21]:

$$\bar{u}_i \bar{u}_j = \tau_{ij} + \bar{u}_i \bar{u}_j \quad (3)$$

Where,  $\tau_{ij}$  is the residual stress tensor. Hence the filtered Navier-Stokes equations can be written as:

$$\frac{\partial \bar{u}_i}{\partial t} + \frac{\partial (\bar{u}_i \bar{u}_j)}{\partial x_j} = -\frac{\partial \bar{p}}{\rho \partial x_i} + 2\nu \frac{\partial}{\partial x_j} \bar{S}_{ij} - \frac{\partial \tau_{ij}}{\partial x_j} \quad (4)$$

Unclosed residual stress tensor ( $\tau_{ij}$ ) in Eq. (4) can be modelled using different subgrid-scale models. In this study, Smagorinsky-Lilly subgrid-scale model was used and the governing equations can be written as [22]:

$$\tau_{ij} - \frac{1}{3} \tau_{kk} \delta_{ij} = -2\mu_t \bar{S}_{ij} \quad (5)$$

$$\mu_t = \rho L_s^2 |\bar{S}| \quad (6)$$

$$L_s = \min(kd, C_s \Delta) \quad (7)$$

$$\bar{S} = \sqrt{2S_{ij}S_{ij}} \quad (8)$$

In Eq. (7)  $L_s$  denotes the mixing length for subgrid-scales which is computed using the von Karman constant ( $k$ ) and distance to the closest wall ( $d$ ).

$C_s$ ,  $\mu_t$ ,  $\rho$  and  $\Delta$  in Eqs. (5-7) are the model constant, eddy viscosity, density and cube root of the local grid cell volume, respectively. In LES turbulence model, the value of  $C_s$  is generally in the range of 0,1-0,2.

GAMBIT (ANSYS) was used to create and mesh the numerical domain, which is composed of a rectangular channel and installed vanes (Figure 1).

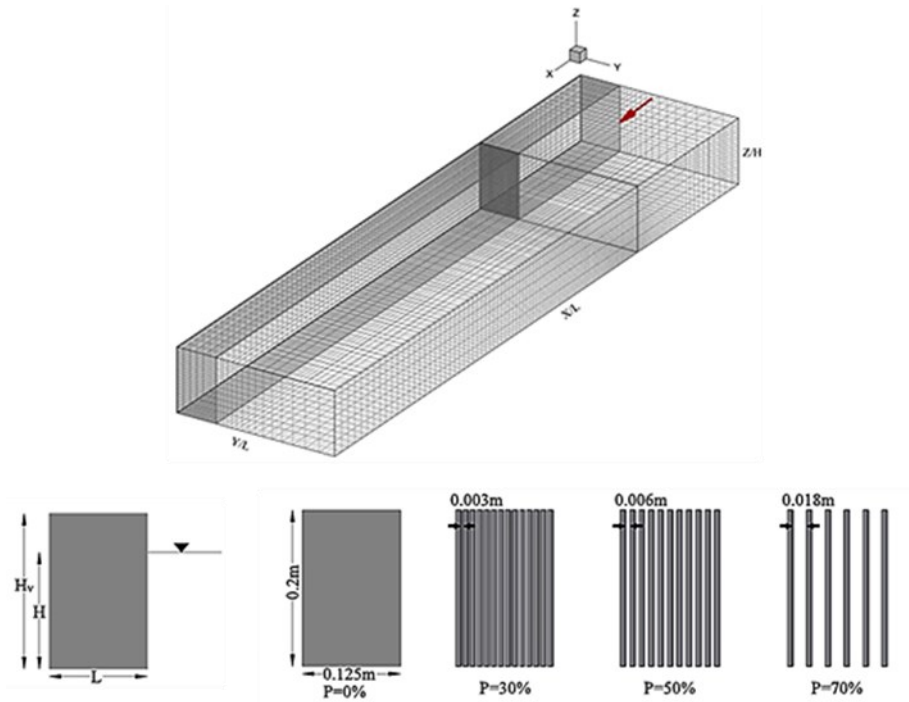


**Figure 1. Numerical domain and tested vanes**

Different permeability rates were adjusted using cylindrical tubes of 6mm diameter. A quad-map mesh was generated for all simulated models.

In this study,  $\frac{K_{res}}{K_{res}+K_{sgs}} > 0,8$  ratio was used to evaluate the generated mesh sufficiency [23]:

$$K_{res} = \frac{1}{2}(\overline{u^2} + \overline{v^2} + \overline{w^2}) \tag{9}$$

$$K_{sgs} = \left(\frac{\mu_{sgs}}{\rho C_s \Delta}\right)^2 \tag{10}$$

Where  $K_{res}$  is the turbulent kinetic energy from resolved velocity fluctuations,  $K_{sgs}$  is the subgrid-scale turbulent kinetic energy and  $\mu_{sgs}$  is the subgrid-scale viscosity.

Because the turbulent kinetic energy ratio was  $\geq 0,9$  in most of the numerical domain, therefore a mesh composed of approximately 154.000 elements was considered as an optimum mesh for all created models to simulate the flow field around the bank-attached vanes. However, it must be noted that it is not possible to generate the mentioned optimum mesh in all cases due to the different permeability rates.

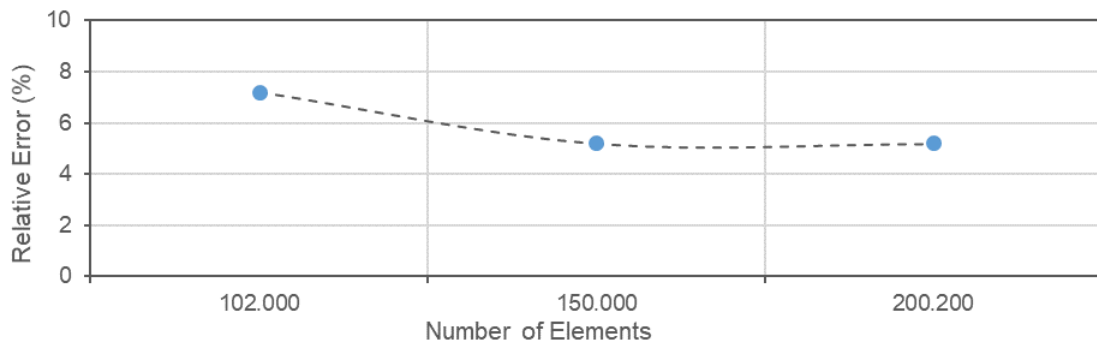


**Figure 2. Average relative error of simulated and measured water surface profiles at different Y/L positions**

Moreover, a mesh independence test for 30 % permeable vane was performed. Simulated and measured water surface profiles at different Y/L positions around 30 % permeable vane showed negligible difference with increasing number of nodes. The average relative error (ARE) for the meshes composed of 150.000-200.200 elements was approximately 5,19 % (Figure 2). Average relative error was calculated using Eq. (11):

$$ARE = \frac{X_{Exp} - X_{Num}}{X_{Exp}} \cdot 100 \tag{11}$$

Where,  $X_{Exp}$  and  $X_{Num}$  are the experimental and numerical water surface profile values.

**Table 1. Hydraulic and boundary conditions**

Hydraulic Conditions	flow depth (m)	approach velocity (m/s)	Fr	Re
		0,15	0,66	0,54
Boundary Conditions	inlet	side walls and vanes	top	outlet
	pressure inlet	wall	pressure inlet	pressure outlet

In this study, LES turbulence model along with volume of fluid (VOF) and SIMPLE scheme was used to resolve the flow field around the bank-attached vanes. Hydraulic and boundary conditions are shown in Table 1.

**2.2 Data validation**

Streamwise free surface profile measurements around 30 % permeable vane were conducted using point gauges of 0,1 mm accuracy in a straight 10 m long and 0,5 m wide rectangular flume located at the Hydraulics Laboratory of the University of Tabriz.

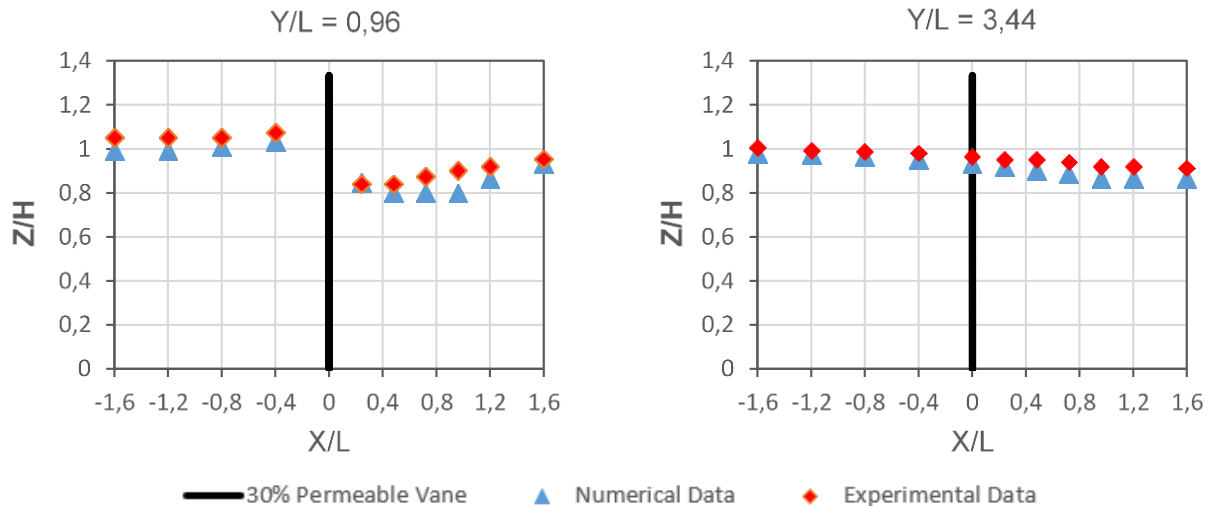


**Figure 3. Numerical and experimental free surface comparison**

To evaluate the accuracy of the numerical model, measured and simulated free surface profiles were compared at the vane tip (Y/L = 0,96) and near the opposite side wall (Y/L = 3,44). Water surface fluctuations at the vane tip is mainly due to the mean pressure and velocity variations which will gradually diminish further downstream. Generally, as shown in Figure 3, experimental and numerical free surface profiles agreed well because the ARE values were approximately 4,7 %. Furthermore, root mean square error (RMSE) of the

experimental and numerical free surface profile values is approximately 0,0072, which indicates that numerical model values are consistent with the experimental results. RMSE was calculated using the Eq. (12), where n is number of the data:

$$RMSE = \sqrt{\frac{\sum_{i=1}^n (X_{Exp} - X_{Num})^2}{n}} \tag{12}$$

### 3 Results and discussion

Depth-averaged velocity variations in the flow field revealed the presence of two flow zones that were formed and developed along the channel due to the local effect of the vane structure and channel cross sectional constriction (Figure 4). These zones are main flow field, upstream and downstream separation regions. The boundary between these zones is called detached shear layer, which is a turbulent-dynamic flow. In the upstream of the vanes and along the side wall, especially near the impermeable vane,  $-1 \leq X/L \leq 0$ , backwater effect is obvious, which affected the local flow characteristics and caused velocity reduction in this region. Velocity increase at the  $X/L=0$  section is due to the channel constriction, which is significant in the impermeable case. Results showed that maximum velocity occurred in the downstream zones due to the flow deflection, formation of the different vortices, secondary flows and their subsequent effect on flow field, on average, the maximum velocity values are 1,54 times the approach velocity ( $V_{app}$ ). Generally, complexity of the flow field in the downstream region due to the presence of the mentioned factors is obvious in the velocity distributions. Maximum velocity decreases up to 11 % for the 70 % permeable vane.

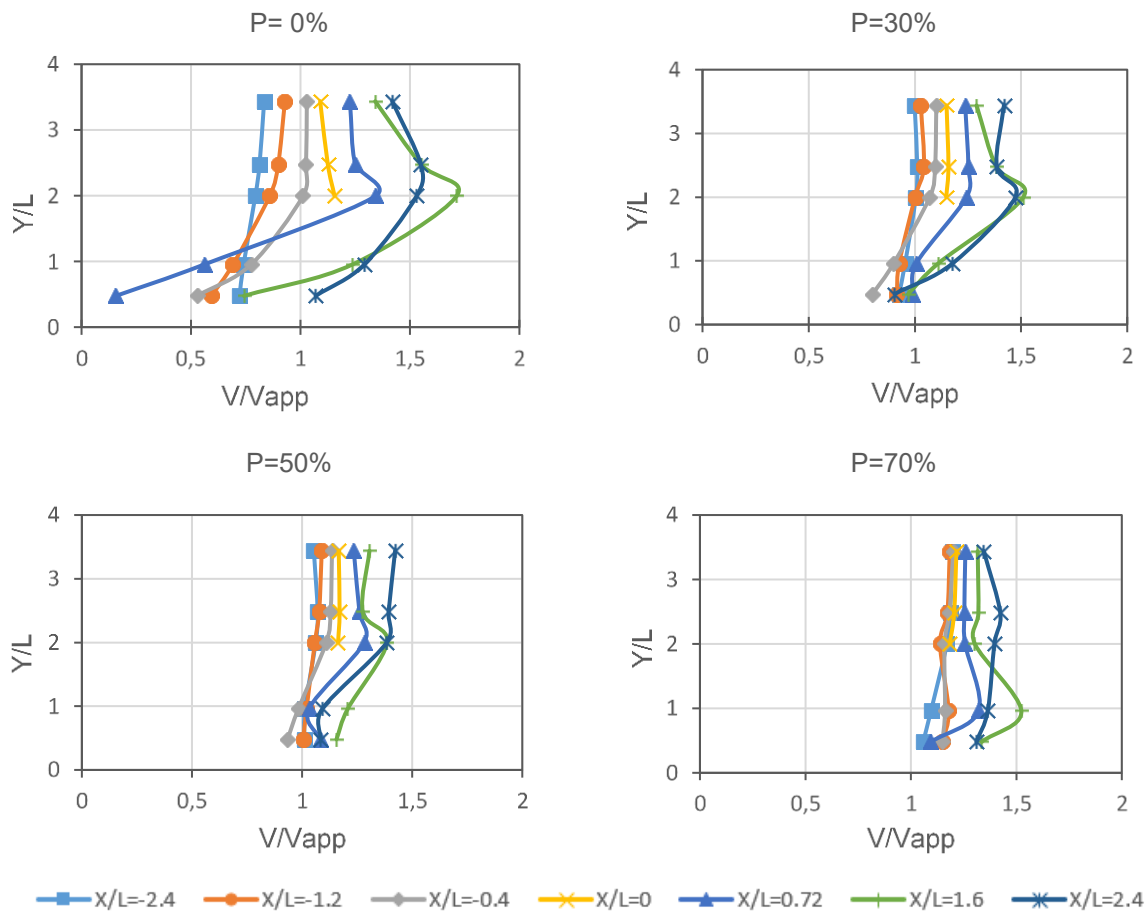


Figure 4. Numerical and experimental free surface comparison

Moreover, in the permeable vanes, small-scale high velocity zones formed within the cylindrical tubes intervals due to the constriction.

Phenomena such as formation of scour hole and structure undermining are developed due to the high velocity zone near the vanes tip region, the tip velocity variation at the  $Z/H=0,03$  is presented in Table 2. Generally, tip velocity ratio ( $V_{tip}/V_{app}$ ) decreases as the permeability rate increases. Tip velocity decreases up to 30,6 % for the 70,0 % permeable vane.

Furthermore, as seen in Table 2, tip velocity ratio results obtained from the LES model are consistent with experimental study of Kang et al. [13], and the slight differences are due to the different hydraulic and geometry conditions.

**Table 2. Comparison of the tip velocity values obtained from LES model with the experimental results of Kang et al. [13]**

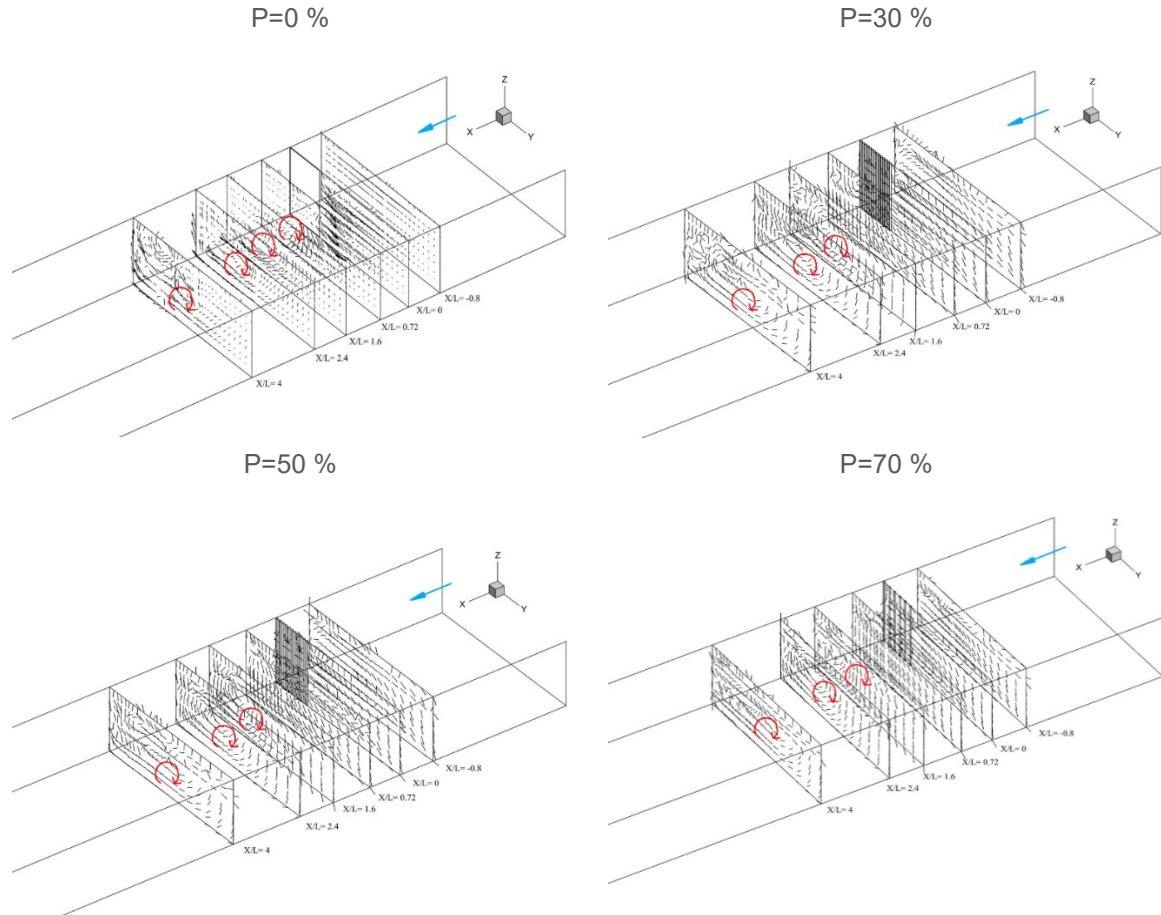
Reference	Structure Type	Method	Flow Depth (m)	$V_{app}$ (m/s)	$V_{tip}/V_{app}$
Kang et al. [13]	Pile Row 0%	ADV LSPIV	0,15	0,40	1,52
	Pile Row 40%				1,25
	Pile Row 60%				1,20
	Pile Row 80%				1,12
Present study	Rec 0%	LES	0,15	0,66	1,84
	Rec 30%				1,49
	Rec 50%				1,35
	Rec 70%				1,28

Figure 5 illustrates secondary flow vectors in the upstream and downstream regions at six different vertical planes, which can be used to analyse the three-dimensional flow structure in the flow field. In the upstream of all the simulated vanes, transverse flow is dominant which generally moves from right side wall of the channel towards the left side wall as a result of longitudinal pressure gradient generated due to the presence of vanes. Furthermore, as flow reaches close to the upstream face of the vanes, the transverse flow amplifies and the highest values occur mainly at the  $X/L=0$ . In the downstream of the vanes, different wakes and vortices are formed, at the  $X/L=0,72$  plane, close to the impermeable vane, relatively strong and stable vortices formed close to the flow separation zone. Note that these vortices do not form immediately downstream of the permeable vanes.

Formation of the vortices along the downstream region of all the simulated vanes  $1,6 \leq X/L \leq 4$ , can be attributed to the different flow deflection at the near bed and upper layers. These vortices gradually move towards the channel centreline with a decrease in the impact of vanes on the flow field. Generally, turbulence generated in the shear layer, is due to the interaction of different wakes and vortices in the flow field. The results indicate that permeable vanes generate weaker vortices along the channel in comparison to the impermeable vane. Further downstream and similar to the  $X/L=-0,8$  section, as vortices gradually diminish, transverse flows form towards the left side wall.

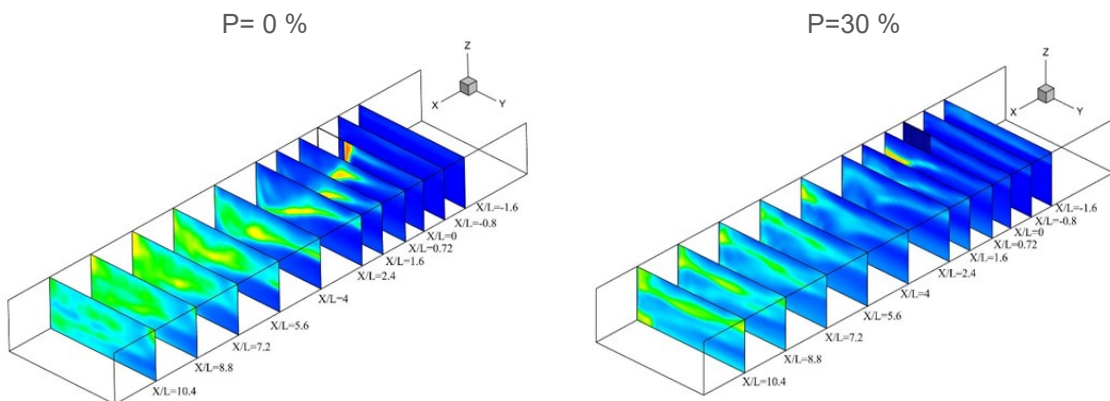
Formation of the wakes, eddies and turbulence effects the recirculation zone characteristics and sedimentation process in the flow field, turbulent kinetic energy (TKE) variations are presented in Figure 6. TKE is generally dominant along the detached shear layer due to the effect of the velocity fluctuations in this region. Relatively intense turbulence patches along the detached shear layer and within the recirculation zone are formed due to the turbulence and subsequent interactions of the different wakes and vortices such as horseshoe vortices in the flow field. Maximum TKE values within turbulence patches decrease up to 58 % around the 70 % permeable vane. The mean kinetic energy (KE) variations are presented in Figure 7. In the upstream region of the vanes ( $-1,6 \leq X/L \leq -0,8$ ), especially in the impermeable case, decrease in approach flow velocity and formation of backwater close to the bed along the right side wall of the channel is obvious. Downstream of the structures, in the recirculation zone close to the

channel side wall and vanes structure,  $0,72 \leq X/L \leq 10,4$ , the lowest mean KE occurred and extended towards the end of the flow field, but gradually increased towards the left side wall. Comparison of the KE contours showed that, maximum KE decreases up to 43,3 % for the 70 % permeable vane.



**Figure 5. Secondary flow vectors at different vertical planes**

Furthermore, for impermeable and permeable vanes, maximum KE occurred at the  $X/L=2,4$  and  $5,6 \leq X/L \leq 10,4$ , respectively. Generally, due to the dominant effect of the velocity fluctuations and mean flow velocity in the recirculation zone and main flow field, TKE and KE contours are different.



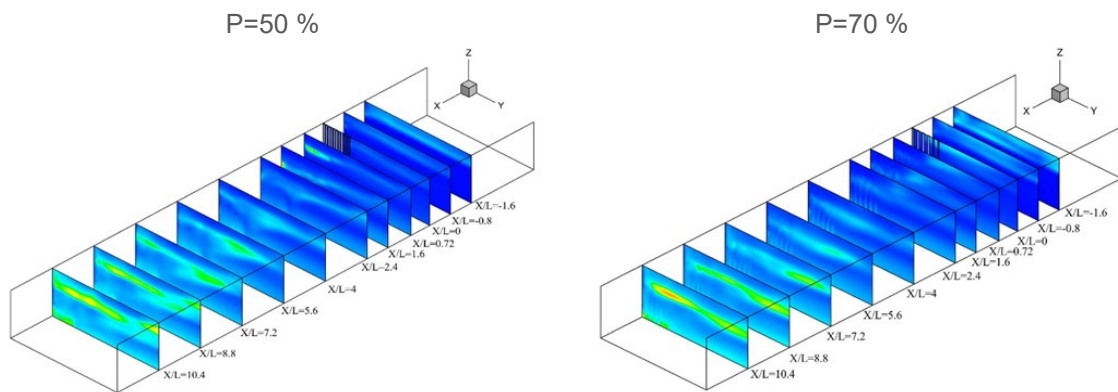


Figure 6. TKE variations in the flow field

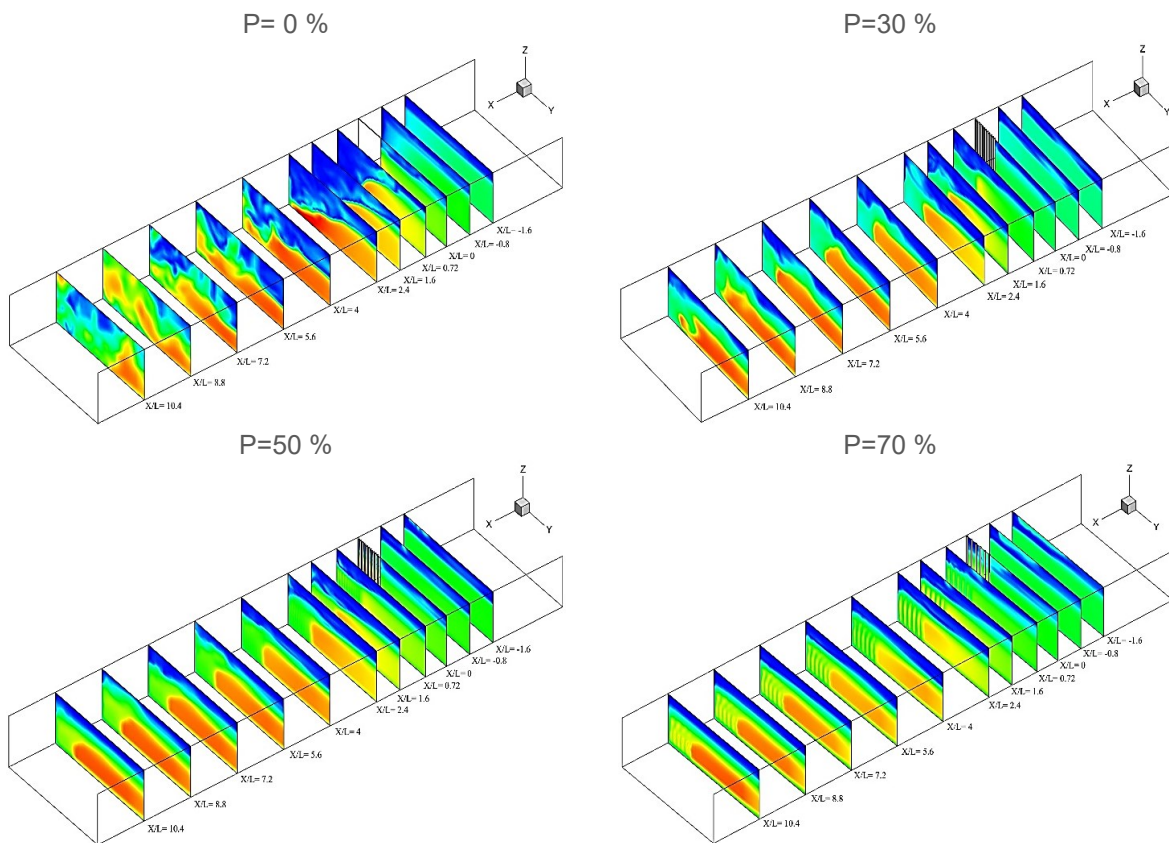


Figure 7. KE variations in the flow field

#### 4 Conclusions

In this study, LES turbulence model was used to simulate the flow field around the bank-attached vanes. Numerical domain was composed of approximately 154.000 elements, because when the number of nodes was increased, the ARE was constant and approximately 5,19 %. Generally, small-scale numerical domain was considered to avoid large mesh

numbers. The accuracy of the numerical model was assessed by comparing the experimental and numerical free surface values. The ARE value was approximately 4,7 %.

Formation and development of two different zones in the flow field can be attributed to the presence of the bank-attached vanes. Interaction of the different wakes and vortices, such as vortex shedding and horseshoe vortices, affected the flow pattern and characteristics such as depth-averaged velocity distribution in these zones. Maximum velocity decreased up to 11 % for the 70 % permeable vane; maximum values mainly occurred in  $1,6 \leq X/L \leq 2,4$  region.

The tip velocity for impermeable vane was approximately  $1,84V_{app}$  whereas it reduced to  $1,28V_{app}$  for 70 % permeable vane.

Different wakes and vortices were dominant in the  $0,72 \leq X/L \leq 4,00$  region.

TKE and KE contours at different vertical planes along the flow field showed that different permeability rates effect the recirculation zone characteristics and sediment deposition process around the vanes. Maximum mean KE occurred for all cases in the downstream region,  $2,4 \leq X/L \leq 10,4$ .

Generally, for a multipurpose design such as creating the riparian habitats, controlling the local flow and secured flow depth for navigation, permeable vanes are appropriate because weaker wakes and vortices form around them. However, still more research is needed to study the variation of other parameters such as pressure and shear stress, understand the three-dimensional nature of the flow affected by different geometries or orientation angles and find the optimal design in accordance with different hydraulic conditions, considering that with higher permeability rates, these structures do not have a noticeable effect on the flow pattern and the decrease in velocity around river banks.

## Acknowledgments

This study was conducted at the University of Tabriz. The authors have no relevant financial or non-financial interests to disclose and no funding was received for conducting this study.

## References

- [1] Hey, R. D. Environmentally sensitive river engineering. In: *The Rivers Handbook: Hydrological and Ecological Principles, Two*, Calow, P.; Petts, G. E. (eds.). River Restoration. Oxford, UK: Blackwell Science; 1996, pp. 80-105. <https://doi.org/10.1002/9781444313871.ch18>
- [2] Rosgen, D. L. The Cross-Vane, W-Weir and J-Hook Vane Structures...Their Description, Design and Application for Stream Stabilization and River Restoration. In: *Proceedings of the 2001 Wetlands Engineering and River Restoration Conference*, Hayes, D. F. (ed.). August 27-31, 2001, Reno, Nevada, USA, ASCE Library; 2001, pp. 1-22. [https://doi.org/10.1061/40581\(2001\)72](https://doi.org/10.1061/40581(2001)72)
- [3] Pagliara, S.; Kurdistani, S. M. Flume experiments on scour downstream of wood stream restoration structures. *Geomorphology*, 2017, 279 (2), pp. 141-149. <https://doi.org/10.1016/j.geomorph.2016.10.013>
- [4] Yeo, H. K.; Kang, J. G.; Kim, S. J. An experimental study on tip velocity and downstream recirculation zone of single groynes of permeability change. *KSCCE Journal of Civil Engineering*, 2005, 9 (1), pp. 29-38. <https://doi.org/10.1007/BF02829094>
- [5] Bhuiyan, F.; Hey, R. D.; Wormleaton, P. R. Bank-Attached Vanes for Bank Erosion Control and Restoration of River Meanders. *Journal of Hydraulic Engineering*, 2010, 136 (9), pp. 583-596. [https://doi.org/10.1061/\(ASCE\)HY.1943-7900.0000217](https://doi.org/10.1061/(ASCE)HY.1943-7900.0000217)
- [6] Tingsanchali, T.; Maheswaran, S. 2-D Depth-Averaged Flow Computation near Groyne. *Journal of Hydraulic Engineering*, 1990, 116 (1), pp. 71-86. [https://doi.org/10.1061/\(ASCE\)0733-9429\(1990\)116:1\(71\)](https://doi.org/10.1061/(ASCE)0733-9429(1990)116:1(71))
- [7] Ettema, R.; Muste, M. Scale Effects in Flume Experiments on Flow around a Spur Dike in Flatbed Channel. *Journal of Hydraulic Engineering*, 2004, 130 (7), pp. 635-646. [https://doi.org/10.1061/\(ASCE\)0733-9429\(2004\)130:7\(635\)](https://doi.org/10.1061/(ASCE)0733-9429(2004)130:7(635))

- [8] McCoy, A.; Constantinesc, G.; Webber, L. J. Numerical Investigation of Flow Hydrodynamics in a Channel with a Series of Groynes. *Journal of Hydraulic Engineering*, 2008, 134 (2), pp. 157-172. [https://doi.org/10.1061/\(ASCE\)0733-9429\(2008\)134:2\(157\)](https://doi.org/10.1061/(ASCE)0733-9429(2008)134:2(157))
- [9] Duan, J. G.; He, L.; Fu, X.; Wang, Q. Mean flow and turbulence around an experimental spur dike. *Advances in Water Resources*, 2009, 32 (12), pp. 1717-1725. <https://doi.org/10.1016/j.advwatres.2009.09.004>
- [10] Brevis, W.; García-Villalba, M.; Niño, Y. Experimental and large eddy simulation study of the flow developed by a sequence of lateral obstacles. *Environmental Fluid Mechanics*, 2014, 14 (4), pp. 873-893. <https://doi.org/10.1007/s10652-013-9328-x>
- [11] Xuelin, T.; Ding, X.; Chen, Z. Large eddy simulations of three-dimensional flows around a spur dike. *Tsinghua Science and Technology*, 2006, 11 (1), pp. 117-123. [https://doi.org/10.1016/S1007-0214\(06\)70164-X](https://doi.org/10.1016/S1007-0214(06)70164-X)
- [12] Yazdi, J.; Sarkardeh, H.; Azamathulla, H. Md.; Ghani, A. Ab. 3-D simulation of flow around a single spur dike with free-surface flow. *International Journal of River Basin Management*, 2010, 8 (1), pp. 55-62. <https://doi.org/10.1080/15715121003715107>
- [13] Kang, J.; Yeo, H.; Kim, S.; Ji, U. Permeability effects of single groin on flow characteristics. *Journal of Hydraulic Research*, 2011, 49 (6), pp. 728-735. <https://doi.org/10.1080/00221686.2011.614520>
- [14] Fang, H; Bai, J.; He, G.; Zhao, H. Calculations of Nonsubmerged Groin Flow in a Shallow Open Channel by Large-Eddy Simulation. *Journal of Engineering Mechanics*, 2014, 140 (5). [https://doi.org/10.1061/\(ASCE\)EM.1943-7889.0000711](https://doi.org/10.1061/(ASCE)EM.1943-7889.0000711)
- [15] Shen, S. et al. Numerical simulation on optimization scheme of permeable hole of permeable sheet piling spur dike. *IOP Conference Series: Earth and Environmental Science*, 2019, 304, 052074. <https://doi.org/10.1088/1755-1315/304/5/052074>
- [16] Ferro, V. et al. Scour around a Permeable Groin Combined with a Triangular Vane in River Bends. *Journal of Irrigation and Drainage Engineering*, 2019, 145 (3). [https://doi.org/10.1061/\(ASCE\)IR.1943-4774.0001380](https://doi.org/10.1061/(ASCE)IR.1943-4774.0001380)
- [17] Abdou, S. S.; ElMoustafa, A. M.; Samy, M. Assessing Flow Bends in Open Channels. *International Research Journal of Advanced Engineering and Science*, 2021, 6 (2), pp. 49-54.
- [18] Iqbal, S. et al. Flow dynamics around permeable spur dike in a rectangular channel. *Arabian Journal for Science and Engineering*, 2021, 46, pp. 4999-5011. <https://doi.org/10.1007/s13369-020-05205-y>
- [19] Haider, R. et al. Flow Characteristics Around Permeable Spur Dike with Different Staggered Pores at Varying Angles. *Arabian Journal for Science and Engineering*, 2022, 47, pp. 5219-5236. <https://doi.org/10.1007/s13369-021-06435-4>
- [20] Mostafa, M. M.; Ameen, A. M.; Mohamed, H. I.; Ahmed, H. S. Optimal flow pattern around hybrid groins with various orientations to improve fish habitat via Experimental Investigation using Acoustic Doppler Velocimeter. *SVU-International Journal of Engineering Sciences and Applications*, 2023, 4 (2), pp. 98-106. <https://doi.org/10.21608/svusr.2023.189730.1096>
- [21] Leonard, A. Energy cascade in large-eddy simulations of turbulent fluid flows. *Advances in Geophysics*, 1975, 18 (Part A), pp. 237-248. [https://doi.org/10.1016/S0065-2687\(08\)60464-1](https://doi.org/10.1016/S0065-2687(08)60464-1)
- [22] Smagorinsky, J. General circulation experiments with the primitive equations. I. The basic experiment. *Monthly Weather Review*, 1963, 91 (3), pp. 99-164. [https://doi.org/10.1175/1520-0493\(1963\)091%3C0099:GCEWTP%3E2.3.CO;2](https://doi.org/10.1175/1520-0493(1963)091%3C0099:GCEWTP%3E2.3.CO;2)
- [23] Gant, S. E. Quality and reliability issues with large-eddy simulation, Report RR656, Health and Safety Executive, UK, 2008, pp. 30-32.